Matter and Radiation at Extremes

RESEARCH ARTICLE

scitation.org/journal/mre

Spectrum-tailored random fiber laser towards ICF laser facility

Cite as: Matter Radiat. Extremes 8, 025902 (2023); doi: 10.1063/5.0129434
Submitted: 5 October 2022 • Accepted: 21 December 2022 •
Published Online: 26 January 2023

Mengqiu Fan,[1,2] Shengtao Lin,[3] Ke Yao,[1] Yifei Qi,[3] Jiaojiao Zhang,[3] Junwen Zheng,[1] Pan Wang,[3] Longqun Ni,[3] Xingyu Bao,[3] Dandan Zhou,[1] Bo Zhang,[1] Kaibo Xiao,[1] Handing Xia,[1] Rui Zhang,[1] Ping Li,[1] Wanguo Zheng,[1] and Zinan Wang[3,a)]

AFFILIATIONS

[1] Laser Fusion Research Center, China Academy of Engineering Physics, Mianyang 621900, China
[2] Graduate School of China Academy of Engineering Physics, Beijing 100193, China
[3] Key Laboratory of Optical Fiber Sensing and Communications, University of Electronic Science and Technology of China, Chengdu 611731, China

[a)] **Author to whom correspondence should be addressed:** znwang@uestc.edu.cn

ABSTRACT

Broadband low-coherence light is considered to be an effective way to suppress laser plasma instability. Recent studies have demonstrated the ability of low-coherence laser facilities to reduce back-scattering during beam–target coupling. However, to ensure simultaneous low coherence and high energy, complex spectral modulation methods and amplification routes have to be adopted. In this work, we propose the use of a random fiber laser (RFL) as the seed source. The spectral features of this RFL can be carefully tailored to provide a good match with the gain characteristics of the laser amplification medium, thus enabling efficient amplification while maintaining low coherence. First, a theoretical model is constructed to give a comprehensive description of the output characteristics of the spectrum-tailored RFL, after which the designed RFL is experimentally realized as a seed source. Through precise pulse shaping and efficient regenerative amplification, a shaped random laser pulse output of 28 mJ is obtained, which is the first random laser system with megawatt-class peak power that is able to achieve low coherence and efficient spectrum-conformal regenerative amplification.

I. INTRODUCTION

Laser plasma instability (LPI), which is caused by the nonlinear effects of laser–plasma interaction, is a major impediment to research into high-energy-density physics, especially laser-driven inertial confinement fusion (ICF).[1] To suppress LPI, three approaches have been proposed: lower laser power density, shorter laser wavelength, and low-coherence laser light. However, for ICF to be successful, the laser pulse energy should be sufficiently high. Owing to the limitations imposed by the focused spot size and the optical materials available for the lasing wavelength, the first two methods are difficult to apply in practice. Thus, low-coherence laser light has come to be regarded as one of the most promising ways to overcome the problem of LPI.[2–4] In fact, starting in the 1990s, laser devices such as Pharos III, Gekko XII, PHEBUS, and Kanal-2 began to explore the use of low-coherence light sources to suppress LPI.[5–8] However, owing to limitations of the laser technologies available at the time, these attempts did not reach their original expectations. At present, the National Ignition Facility (NIF) in the United States, the French Megajoule Facility (LMJ), and a number of facilities in China all adopt for their front-end fiber seed sources 1053 nm single-longitudinal-mode narrow-linewidth fiber lasers together with the use of phase modulation to broaden the spectral bandwidth.[9–11] After phase modulation, the seed light is further decohered by a combination of spatial, temporal, and polarization beam-smoothing techniques, principally continuous phase plates (CPPs), smoothing by spectral dispersion (SSD), and polarization smoothing (PS). On December 5, 2022, the Lawrence Livermore National Laboratory (LLNL) conducted the first controlled fusion experiment at NIF in history to

reach the milestone of scientific energy breakeven.[12] Although the specific technical details have not yet been published, at the press conference held by the Department of Energy (DOE) on December 13, 2022, scientists from LLNL mentioned that NIF had used the cross-beam energy transfer (CBET) method to overcome insufficient driving of the inner ring caused by severe LPI, resulting in a significantly improvement of compression symmetry. In conclusion, suppression of LPI remains a central focus of research aimed at achieving high-gain fusion reactions in laser-driven ICF facilities.

With recent developments in laser technology, an increasing number of investigations are being carried out on laser facilities that directly use low-coherence light sources for amplification, transmission, and frequency conversion.[13–21] In 2019, a team at the Shanghai Institute of Laser Plasma of the China Academy of Engineering Physics (CAEP) proposed the concept of an instantaneous broadband pulse light source. The spectrum of such a light source is broadband in any time slice,[16] and its pulse and spectrum can be independently shaped. On the basis of this approach, the team constructed a low-coherence laser facility with 1 kJ/2ω output, called Kunwu. At the Laboratory for Laser Energetics (LLE) at the University of Rochester, incoherent pulses have been amplified by optical parametric amplification in the infrared (~1053 nm), and broadband sum-frequency generation to the ultraviolet (~351 nm) has been realized.[17–19] However, both of these approaches employed complex spectral shaping methods and amplification routes to simultaneously realize low coherence and high energy.

In 2010, a new type of low-coherence optical fiber light source, namely, the random fiber laser (RFL), was proposed.[22] The essential difference in principle between the RFL and a traditional fiber laser is that the feedback of RFL is provided by the distributed Rayleigh scattering. Therefore, the output laser has no fixed longitudinal mode spacing, and it represents a new type of light source with low coherence.[23,24] Moreover, the output characteristics of the RFL can be adjusted by varying the cavity structure, thus enabling tailored design of RFLs for specific applications.[25–33]

This paper describes the first study of the use of an RFL as the seed source for an ICF driver and achieving efficient amplification, thus providing a basis for further study of RFLs for ICF. With this aim in mind, we first measure the gain spectrum of N31 Nd:glass in a solid laser amplifier, following which we carefully tailor the structure of the RFL. Using nonlinear Schrödinger equations (NLSEs), we construct a theoretical model to provide a comprehensive description of the output characteristics of the proposed RFL, and we perform spectrum tailoring procedures based on this model. Finally, we carry out experimental tests of the whole RFL system. In particular, we obtain a 28 mJ/5 ns squared pulse from the RFL, which is the largest pulse energy and the highest peak power of any RFL to date. Since the spectrum of this RFL matches the solid-state laser amplification medium very well while retaining low coherence, the amplification process is simplified (without the need for complex spectral modulation methods), and hence high-efficiency amplification is achieved. This work demonstrates the good adaptability of RFLs as a new kind of low-coherence seed source for high-power solid-state laser facilities and reveals their promise for applications in ICF and high-energy-density physics.

II. 1053 nm SEED RFL DESIGN

As mentioned above, the main motivation behind RFL design is to realize efficient amplification and obtain high energy output based on the mainstream ICF laser driver configuration. In this section, the characteristics of the amplification system, especially the regenerative amplifier, are analyzed. According to these amplification properties, we design a 1053 nm broadband RFL as a seed laser. We propose a novel simulation model to investigate the RFL output properties, and we introduce a special spectrum tailoring method to achieve a broadband spectrum.

In ICF and other areas of high-energy-density physics research, Nd:glass is the most widely used gain medium to realize high energy amplification. Reference 34 gives the main parameters of Nd:laser glasses (including the N31 Nd:glass that we use) radiating at ~1053 nm for high-peak-power lasers. The theoretical free-oscillation spectrum is plotted as the black curve in Fig. 1. Since the linewidths of presently available phase-modulated lasers are only a few tenths of a nanometer, which is far narrower than the gain bandwidth of Nd:glass, the influence of the gain narrowing effect on the amplification efficiency can basically be ignored. On the other hand, the linewidth of an amplified spontaneous emission (ASE) light source is more than tens of nanometers, which far exceeds the effective gain bandwidth of multipass amplification based on Nd:glass, and hence multiple spectral control means have to be employed to compensate for the gain narrowing effect.

Here, for the first time, we experimentally measured the free-oscillation spectrum of our regenerative amplifier based on an N31 Nd:glass rod in the case of ~140-pass amplification (the actual number with light injection of the order of nanojoules), and the results are shown as the red curve in Fig. 1. The 3 dB free-oscillation spectrum of the regenerative amplifier ranges from 1051.7 to 1054.5 nm, with a total width of about 2.8 nm. It is important to note that the difference between the two curves is mainly due to the fact that the actual Nd:glass gain profile is not the ideal Lorentzian profile. In addition, the gain of the regenerative amplifier decreases more slowly in the longer-wavelength region than in shorter-wavelength region. These experimental measurements can be used to guide the seed laser design by matching the gain spectrum of the regenerative amplifier.

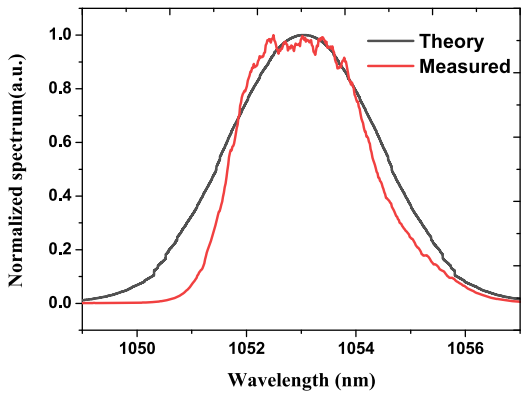

FIG. 1. Free-oscillation spectrum of a regenerative amplifier based on an N31 Nd:glass rod.

An RFL is a novel low-coherence light source with flexible output features that can be tailored by the cavity design, and its output for a fixed structure can exhibit stable time-domain and frequency-domain characteristics,[23,35] which is why RFLs are candidates for use as broadband seed sources in ICF. The emission profile of ytterbium-doped fiber (YDF) covers a wide spectral range from 1.03 to 1.09 μm, and this enables a ytterbium-doped RFL (YRFL) to achieve sufficient emission at the corresponding gain band of Nd:glass. Moreover, the output spectrum of a half-open RFL can be tuned by varying the spectrum of the point feedback and the YDF length. Therefore, in this work, a half-open cavity RFL with the gain from a ytterbium-doped fiber and the random feedback from passive fiber distributed Rayleigh scattering is studied.

In the detailed RFL structure, shown in Fig. 2(a), the YDF is cladding-pumped by a 976 nm laser diode (LD) through a $(2+1)\times 1$ pump combiner; a cladding power stripper (CPS) is connected at the end of the YDF to remove the unabsorbed pump light, and the output of the CPS is attached to several kilometers of HI 1060 FLEX fiber, providing randomly distributed Rayleigh scattering feedback. A fiber loop mirror (FLM) is attached to the 1053 nm port of the wavelength division multiplexer (WDM) to provide wideband point feedback. It should be noted that the WDM is customized and the bandwidth of the WDM 1053 nm port is about 2.6 nm (from 1051.8 to 1054.5 nm), to suit the gain spectrum of the Nd:glass.

A. Simulation model

Based on the proposed setup, a simulation model is constructed for theoretically analyzing the output characteristics of the YRFL. This model starts from the generalized nonlinear Schrödinger equations,[36,37] and it can be divided into two main parts, dealing with simulation of the YDF section and the HI060 FLEX fiber section, respectively.

For the YDF section, the light wave envelopes can be described as

$$\frac{\partial A^+}{\partial z}+\frac{i\beta_2}{2}\frac{\partial^2 A^+}{\partial t^2}+\frac{\alpha}{2}A^+=i\gamma\left(|A^+|^2+2|A^-|^2\right)A^+ +g\left(|A^+|^2+|A^-|^2\right)A^+, \quad (1)$$

$$-\frac{\partial A^-}{\partial z}+\frac{i\beta_2}{2}\frac{\partial^2 A^-}{\partial t^2}+\frac{\alpha}{2}A^-=i\gamma\left(|A^-|^2+2|A^+|^2\right)A^- +g\left(|A^+|^2+|A^-|^2\right)A^-. \quad (2)$$

Here, A is the complex envelope of the RFL light wave, with superscripts + and − corresponding to the forward- and backward-propagating waves, respectively. α, γ, and β_2 are the linear fiber loss, Kerr coefficient, and second-order dispersion. The gain g from the YDF can be expressed as

$$g(P_s^+,P_s^-)=\frac{\alpha_s\mu\frac{P_p(z)}{P_{\rm sat}^{(p)}}+\alpha_s\frac{P^+(z)+P^-(z)}{P_{\rm sat}^{(s)}}}{1+\frac{P^+(z)+P^-(z)}{P_{\rm sat}^{(s)}}+\frac{P_p(z)}{P_{\rm sat}^{(p)}}}, \quad (3)$$

where P is the light-wave power, and

$$\alpha_s=\Gamma_s\sigma_{as}N,\qquad \alpha_p=\Gamma_p\sigma_{ap}N,$$

$$P_{\rm sat}^{(s)}=\frac{h\nu_s A_c}{\tau(\sigma_{as}+\sigma_{es})\Gamma_s},\ P_{\rm sat}^{(p)}=\frac{h\nu_p A_c}{\tau(\sigma_{ap}+\sigma_{ep})\Gamma_p},\ \mu^{-1}=\frac{\sigma_{es}}{\sigma_{ep}}\frac{\sigma_{ap}+\sigma_{ep}}{\sigma_{as}+\sigma_{es}}.$$

Here, Γ_p and Γ_s are the 976 nm pump and 1053 nm emission overlap within the core, respectively. σ_a and σ_e are the absorption and emission cross-sections for the YDF. N is the total number of Yb^{3+} ions integrated over the fiber mode cross-section, and N_2 is the number of excited Yb^{3+} ions. A_c is the core area of the YDF. $\tau=0.8$ ms is the Yb-ion lifetime.

The nonlinear effect in the HI 1060 FLEX fiber section is significantly less than that in the YDF, and the main function of the HI 1060 FLEX fiber is to provide randomly distributed Rayleigh scattering feedback for YRFL formation. Thus, the simulation model for the HI 1060 FLEX fiber mainly describes its Rayleigh scattering process:

$$\frac{\partial u_s^{\pm}}{\partial z}+i\frac{\beta_{2s}}{2}\frac{\partial^2 u_s^{\pm}}{\partial t^2}+\frac{\alpha_s}{2}u_s^{\pm}=\frac{\varepsilon(\omega)}{2}u_s^{\mp}. \quad (4)$$

Here, s indicates the generated RFL emission, ω is the angular frequency of the light wave, and ε is the Rayleigh scattering coefficient. The total length of the YDF is denoted by $L_{\rm YDF}$, and the length of the single-mode fiber (SMF) is denoted by $L_{\rm SMF}$.

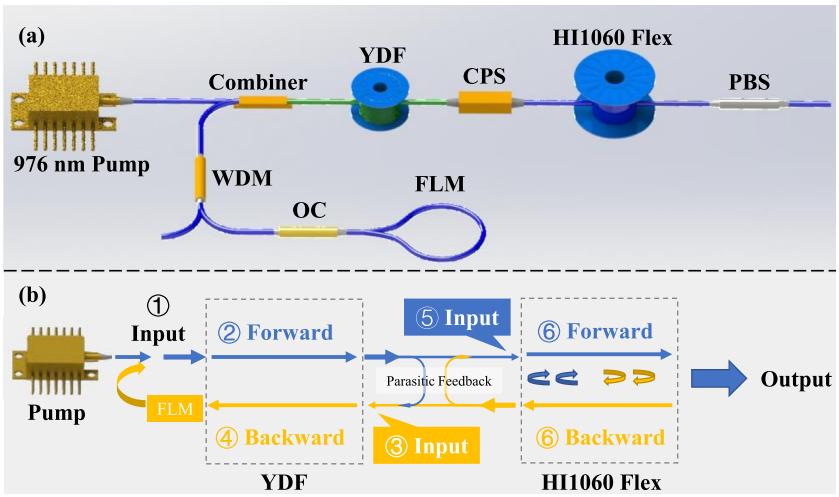

FIG. 2. Experimental setup and corresponding simulation model for YRFL.

We now present the iterative method for modeling the YRFL build-up process in more detail. The specific procedures are shown in Fig. 2(b) and can be described as follows:

① Set the initial values of $A_p^+(0)$ and $A_s^+(0)$. The boundary conditions for the initial values can be expressed as $A_p^+(0) = P_{in}$ and $A_s^+(0) = \sqrt{R_{FLM}}\, A_s^-(0)$, respectively, where $R_{FLM} = 0.6$ is the reflectivity of the fiber loop mirror.
② Insert the initial values into Eq. (1) to obtain the envelope of forward light waves in the YDF. The parameter values for the YDF are listed in Table I.
③ The boundary conditions for backward light waves are $A_p^-(L_{YDF}) = \sqrt{R_{PR}}\, A_p^+(L_{YDF})$ and $A_s^-(L_{YDF}) = \sqrt{R_{PR}}\, A_s^+(L_{YDF}) + u_s^-(L_{YDF})$, where $R_{PR} = 2 \times 10^{-5}$ is the parasitic reflection.
④ Based on the boundary conditions, the envelope of backward light waves in the YDF can be obtained using Eq. (2).
⑤ At the same time, the forward excitation light wave is injected into the HI 1060 FLEX fiber. The boundary condition is $u_s^+(L_{YDF}) = A_s^+(L_{YDF})$.
⑥ The envelope of light waves in the SMF is calculated based on Eq. (4). The transit time is about L_{YDF}/nc, where n is the refractive index of the YDF and c is the speed of light in vacuum, corresponding to the transit time from CPS back to the pump point. The parameter values for HI 1060 FLEX fiber are listed in Table II.

The iterative process from ① to ⑥ is repeated thousands of times until a stable solution is obtained.

B. Spectrum tailoring

Using the simulation model, we performed a series of numerical calculations on the output spectrum and found that the shape of the YRFL spectrum is related to the length of the YDF, as shown in Fig. 3. With a relatively short YDF (~0.5 m), the emission of Yb^{3+} plays a dominant role in the formation of the YRFL spectrum. Therefore, the output spectrum of the YRFL has a similar shape to the Yb^{3+} emission cross-section σ_{es}, i.e., it is a right-sloping spectrum, as shown in Figs. 3(a) and 3(b). With a longer YDF (~5.5 m), the emission light wave is gradually absorbed as it propagates in the YDF, and the output spectrum of the YRFL is affected by the absorption spectrum of the YDF, σ_{as}. Owing to the greater absorption at short wavelengths, the output spectrum of the YDF is left-sloping [Figs. 3(e) and 3(f)]. To achieve a broadband-flat output spectrum, the length of the YDF needs to be optimized. In this work, this length is chosen as 0.9 m, and the resulting output spectrum is shown in Figs. 3(c) and 3(d). The simulation and experimental results all show a flat spectrum with bandwidth ~2.7 nm and ranging from 1051.8 to 1054.5 nm, and the coherence time is about 907 fs. Compared with a previous phase-modulated source,[38] for which the bandwidth was 0.15 nm and the coherence time 16.4 ps, the coherence time of the light source in this work is greatly reduced. The spectrum tailoring is focused on the effective gain bandwidth of N31 Nd:glass, which is theoretically beneficial for efficient amplification. It should be mentioned that all of the above analytical calculations and experiments were based on a 3 km HI 1060 FLEX fiber configuration providing sufficient Rayleigh scattering feedback.

TABLE I. Simulation parameters for YDF.

Parameter	Pump	Emission
λ (nm)	976	1053
σ_a (m^2)	2.48×10^{-24}	2.06×10^{-26}
σ_e (m^2)	2.48×10^{-24}	3.68×10^{-25}
β_2 (s^2/m)	-3×10^{-26}	-2.6×10^{-26}
Γ	0.0064	0.85
α (m^{-1})	0.006	0.004
A_c (m^2)	7.8540×10^{-11}	

TABLE II. Simulation parameters for HI 1060 FLEX fiber.

Parameter	Emission
λ	1053 nm
β_2	1.64×10^{-26} s^2/m
ε	4.3×10^{-6} m^{-1}
α	2.2 dB/km

C. Power performance

According to the above analyses, the lengths of the YDF and the HI 1060 FLEX fiber were chosen as 0.9 m and 3 km, respectively, in our experiment. Figure 4 shows the output YRFL power at the fiber end as a function of 976 nm pump power. In this case, the threshold for the YRFL is about 0.9 W. Above this threshold,

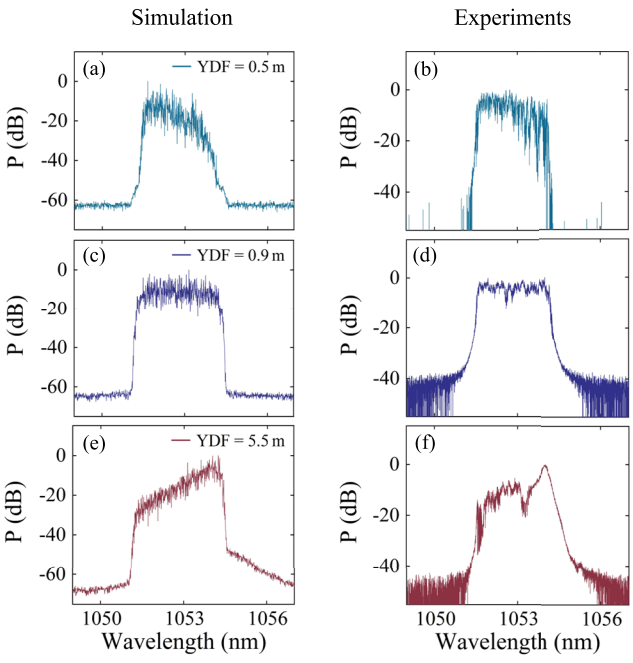

FIG. 3. Output spectrum of the YRFL with different YDF lengths.

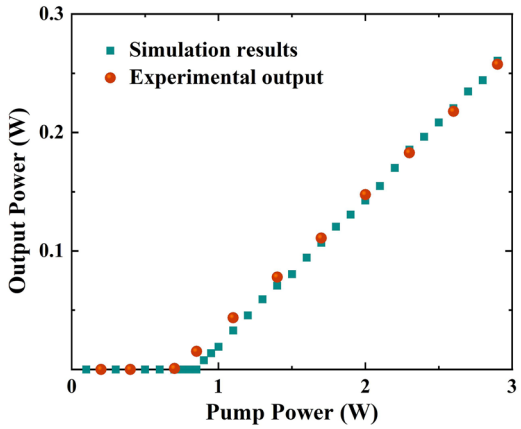

FIG. 4. Output power of the YRFL vs pump power.

the lasing power increases linearly, with a slope efficiency of about 14%. The relative limited optical conversion efficiency is due to the short YDF used in this setup;[39] nevertheless, the seed power is more than enough as the input for subsequent stages. As is clearly shown in Fig. 4, the simulation results are in accord with the experimental results, once again showing the good accuracy of the simulation model.

III. TIME-DOMAIN SHAPING AND FIBER AMPLIFICATION

To obtain an RFL that is able to meet the requirements of regenerative amplifier injection, we also develop an all-fiber front-end system with time-domain shaping and amplification. The system is configured after the RFL seed source with polarization-maintaining fiber (PMF) throughout, as shown in Fig. 5. The output of the RFL seed source is polarized by a polarizing beam splitter (PBS) in order to adapt to the PMF system, and the power output of the PBS is tuned as 16.88 mW. A waveguide amplitude modulator (AM) based on $LiNbO_3$ crystal is used to precisely manipulate the temporal shape of the RFL. An arbitrary waveform generator (AWG) provides radio-frequency (RF) pulse signals with arbitrary shapes for the AM. The AM and AWG together realize the RFL time-domain shaping capability, including pulse shape, pulse duration, and repetition rate.

The shaped RFL pulse is then amplified by two-stage YDF amplifiers, each of which is composed principally of 1.5 m polarization-maintaining YDF (PM-YDF), a circulator, a filter Faraday mirror (FM), a WDM, and a single-mode LD pump. The core diameter of the YDF is 6 μm. The 976 nm LD pump is coupled to the gain fiber core via the WDM. The filter FM consists of a filter and a Faraday rotator mirror, and its main function is to realize axial-alternating PM double-pass fiber amplification. After the first-pass amplification, the laser is reflected back into the gain fiber by the FM, and the polarization direction is rotated by 90° relative to the input polarization direction to compensate for the group delay between the fast and slow axes in the PMF. The purpose of the filter is to filter out the ASE noise generated by the first-pass amplification. When it is reflected and amplified for the second time, the out-of-band ASE generated in the first pass will not deplete the number of particles in the upper energy level, and this not only improves the pumping efficiency, but also effectively improves the signal-to-noise ratio of the output frequency domain of the amplifier. In addition, a filter is connected to the third circulator terminal, which is used to filter out ASE noise generated by the second-pass amplification, and the pulse signal-to-noise ratio is improved again.

Because the fiber front-end system of a high-power laser driver works at a typical repetition frequency of 1 kHz, time-domain ASE noise should be taken into account in addition to frequency-domain ASE noise. In this work, an acoustic optical modulator (AOM) is arranged behind the fiber amplifier, and this can realize a flat-top gated waveform longer than 30 ns, to enable time-domain switching control of laser pulse sequences. The extinction ratio of the AOM is >40 dB. The second-stage amplifier is identical to the first one.

The output energy after the front-end system is greater than 17 nJ with a 5 ns squared pulse. The various time-domain signals and the corresponding spectra of the different pulses are illustrated in Fig. 6. It should be noted that the time-domain signals are detected by a 1 GHz photoreceiver and sampled by a 25 GHz oscilloscope. The stability of the time-domain modulated signals depends on the ratio between the electrical measurement bandwidth E and the optical bandwidth of the signal S. However, owing to the ultrawide bandwidth of the optical signal, the time-domain information is inevitably distorted, and information is lost even with high-precision photoreceivers. To facilitate comparisons of time-domain characteristics with those of other sources intended for use in ICF, namely, the superluminescent diode (SLD) source in Ref. 14 and the ASE source in Ref. 19, for which the E/S ratios are about 0.09% and 0.25%, respectively, an intermediate value of E/S = 0.15% is chosen, and a

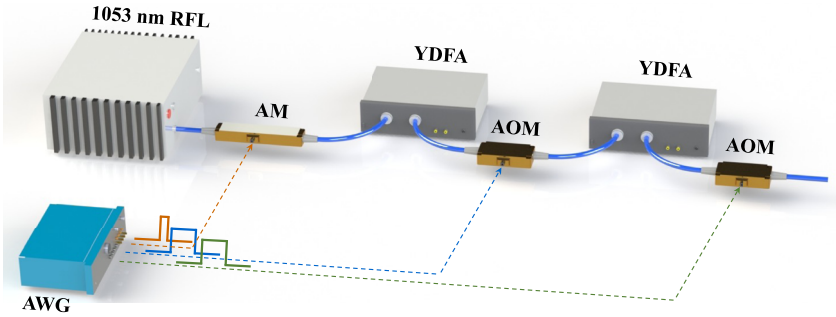

FIG. 5. Experiment setup for time-domain shaping and fiber amplification.

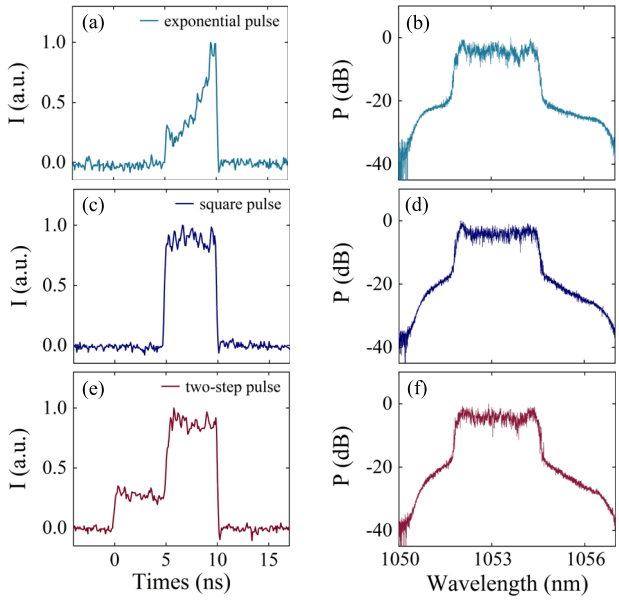

FIG. 6. Pulse shapes after fiber amplification: (a) exponential pulse; (c) square pulse; (e) two-step pulse. The corresponding spectra are shown in (b), (d), and (f).

1 GHz photoreceiver is therefore selected. As shown in Figs. 6(a), 6(c), and 6(e), the time-domain shape is modulated from an exponential pulse to a square pulse, and then to a two-step pulse. There is little spectral filtering effect, owing to the use of a broadband filter with a filtering bandwidth larger than that of the seed random light source. Furthermore, because the fiber amplification system employs an axial-alternating PM double-pass amplification configuration, polarization mode dispersion is well compensated for, and spectral distortion is avoided. Hence, the RFL possesses better spectral stability, as can be seen from Figs. 6(b), 6(d), and 6(f), and the pulse shape remains basically undistorted. The optical signal-to-noise-ratio (OSNR) of the spectrum is as high as 16 dB, and the 3 dB bandwidth is ~2.5 nm. It is worth noting that each spectrum has a wide base, principally because the pulse duty cycle is only 10^{-6}, which will make the ASE manifest during the measurement of the spectrum, but also because, as the laser power increases, nonlinear effects will become stronger, which will broaden the spectrum and reduce the OSNR.

IV. REGENERATIVE AMPLIFICATION

A regenerative amplifier is a promising candidate for preamplification of nanosecond pulses. It is able to achieve a high total gain (10^9) owing to multipass amplification. Meanwhile, the regenerative cavity ensures good beam quality owing to mode self-reproduction. Finally, the gain saturation effect caused by multipass amplification can effectively improve pulse-to-pulse energy stability.[40] Here, we introduced a homemade regenerative amplifier to amplify the nanosecond pulse output from the fiber amplification system.

The random laser pulse is shaped to an exponential, square, or two-step shape and amplified to several tens of nanojoules via the fiber-end system. The shaped pulse is further amplified to the order of millijoules by the homemade regenerative amplifier based on a Nd:glass rod. The regeneration cavity has a concave–convex cavity design with an intracavity lens, and it optical structure is shown in Fig. 7. The regenerative amplifier uses polarization multiplexing technology to improve its energy extraction efficiency, and it achieves high-gain and high-stability amplification through the use of Nd:glass with low gain coefficient. A detailed description of the design of such a regenerative amplifier can be found in Ref. 40. It should be noted that the input energy of the regenerative amplifier used in the present work is different from that in Ref. 40, and hence the system operating parameters are slightly different.

Taking a typical 5 ns square pulse as an example, when the input energy is of the order of nanojoules, the number of amplification passes for the regenerative amplifier is set to ~140, and the pump current is about 137 A. The relationship between the input energy and output energy of the regenerative amplifier is shown in Fig. 8. When the input energy exceeds 4 nJ, the output energy tends to be stable owing to saturation, and when the input energy is 6.28 nJ, the output energy reaches a maximum of 28 mJ at 1 Hz repetition rate. The different time-domain signals and the corresponding spectra of the different pulses are illustrated in Fig. 9. In the regenerative amplifier section, the spectrum of the RFL is carefully designed according to the gain spectrum of the Nd:glass used in the regenerative amplifier, which effectively compensates for the gain narrowing

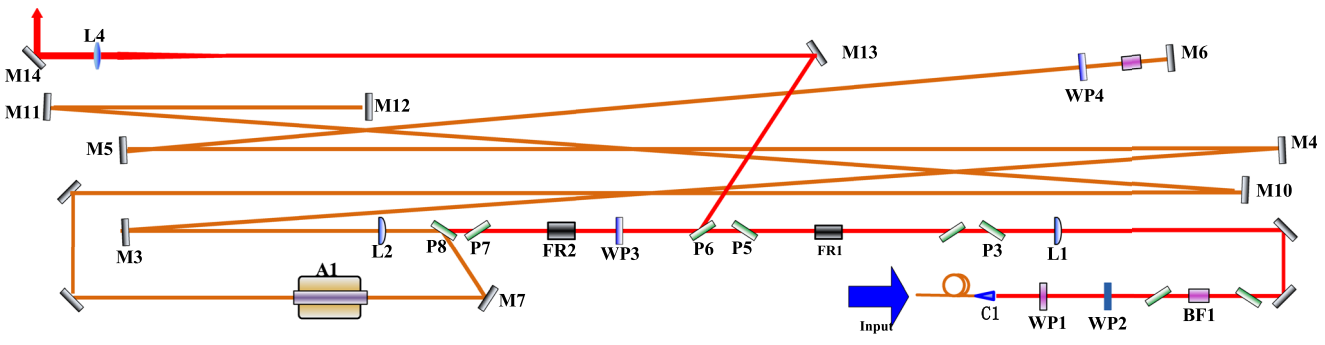

FIG. 7. Experimental setup of regenerative amplifier.

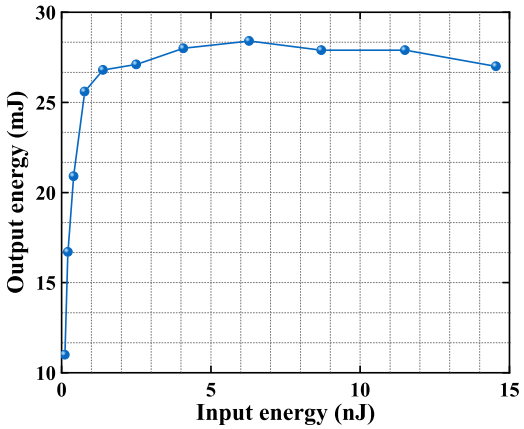

FIG. 8. Energy curve of regenerative amplification.

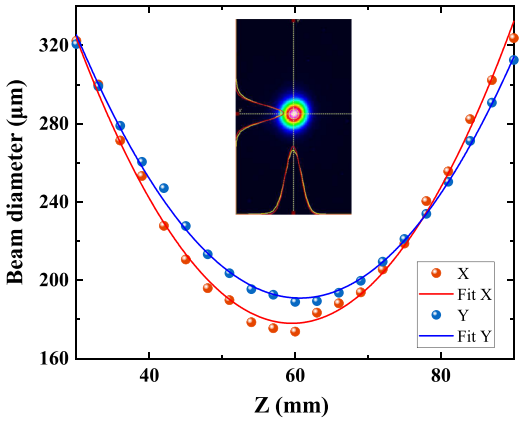

FIG. 10. Measured beam quality after regenerative amplification.

effect during the regenerative amplification. The OSNR of the spectrum is as high as 12 dB, and the 3 dB bandwidth is 2.5 nm according to the smoothed spectral profile. Although the spectral bandwidth of the RFL is not significantly reduced, the hundreds of passes through the regenerative amplifier smooth the rectangular spectral edges of the RFL owing to the residual gain narrowing effect. Even so, the time-domain pulse shape before and after the regenerative amplification still remains relatively stable, as can be seen by a comparison of Figs. 6 and 9, which additionally shows that RFL is also an instantaneous broadband light source.[14] In other words, the distribution of spectral components is time-dependent, and the spectral distortion in the amplification process will not change the time-domain shape.[35,41] Finally, the beam quality of the amplified laser is measured by using a CCD camera after the output port. The output beam is shown in Fig. 10, from which it can be seen that it exhibits a Gaussian distribution, and a beam quality of M_x^2 = 1.15 and M_y^2 = 1.16 is measured with the $1/e^2$ method. Besides, the beam quality in this work is basically consistent with previous results[40] obtained using phase-modulated seed light sources.

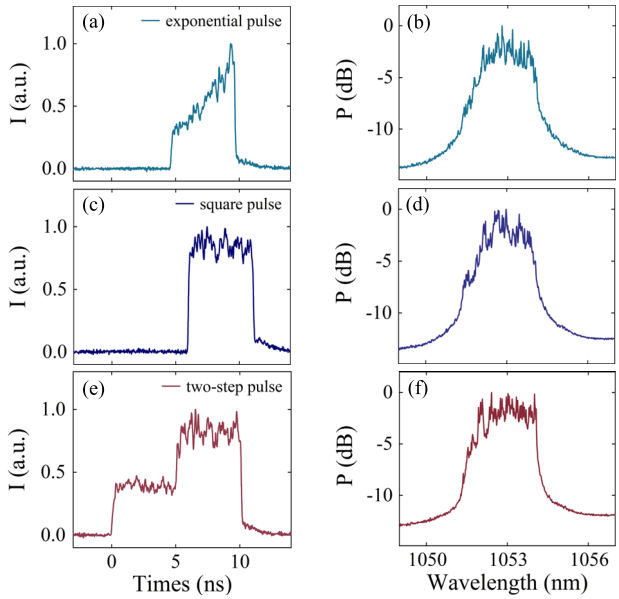

FIG. 9. Pulse shapes after regenerative amplification: (a) exponential pulse; (c) square pulse; (e) two-step pulse. The corresponding spectra are shown in (b), (d), and (f).

V. DISCUSSION AND CONCLUSIONS

Uniform implosion compression is the fundamental requirement for ICF to achieve its ignition target.[42] Whether through enlarging the energy scale of a laser facility or introducing various beam smoothing methods, the main aim is to inject more energy into the hohlraum and improve the implosion compression ratio. Although an ASE source with a tens of nanometer spectral width can greatly reduce temporal coherence,[43] its output energy is several orders of magnitude lower than that of a phase-modulated source, owing to the limitations imposed by the gain bandwidth and the amplification mode of solid-state amplifiers. The spike trains of uneven duration and delay (STUD) pulse scheme reduces the interaction time between laser and plasma hot spot, by controlling the "on" and "off" of each pulse in the sequence of laser pulses, thus facilitating LPI suppression. However, to ensure sufficient output energy, the average intensity over the spike duration equals that of a continuous pulse, while the peak intensity of the spike is increased by a significant factor with regard to the duty cycle.[44] This imposes extremely stringent requirements on the load and damage performance of the final optics.

Because of its unique feedback mechanism, an RFL seed source can achieve low coherence with a several nanometer spectrum by appropriate cavity design. In this work, a spectrum-tailored RFL has been designed and built, and its applicability with pulse shaping and solid-state medium amplification has been experimentally verified. A 28 mJ pulse energy and a megawatt-level peak power have been achieved, marking a new record for an RFL. Compared with a phase-modulated pulse, the RFL pulse has continuous spectral components with a random phase distribution, which is more beneficial to LPI suppression. Moreover, since the laser bandwidth can be well

matched with the solid-state laser amplification medium, and the final optics load requirement can be reduced while ensuring sufficient output energy, if the gain bandwidth of the solid-state amplifier allows, then the spectral width of the RFL could be further increased by the use of different cavity designs. Thus, as a new type of high-power laser driver seed source, the RFL has considerable scientific merit and good prospects for practical application.

ACKNOWLEDGMENTS

The authors are grateful for the support of the National Natural Science Foundation of China (Grant Nos. 62075030, 62075201, and 11904339) and the Sichuan Provincial Project for Outstanding Young Scholars in Science and Technology (Grant No. 2020JDJQ0024). The authors would also like to thank Song Gao, Xiaocheng Tian, Xiangjun Xiang, and Mengjie Lv for their help with the experiment and for fruitful discussions.

AUTHOR DECLARATIONS

Conflict of Interest

The authors have no conflicts to disclose.

Author Contributions

M.F. and S.L. contributed equally to this work.

Mengqiu Fan: Conceptualization (lead); Formal analysis (equal); Validation (lead); Writing – original draft (lead); Writing – review & editing (lead). **Shengtao Lin**: Formal analysis (equal); Validation (lead); Writing – original draft (lead); Writing – review & editing (lead). **Ke Yao**: Formal analysis (supporting); Methodology (supporting); Validation (supporting); Writing – review & editing (equal). **Yifei Qi**: Formal analysis (supporting); Validation (equal); Writing – original draft (equal); Writing – review & editing (supporting). **Jiaojiao Zhang**: Formal analysis (supporting); Validation (supporting); Writing – original draft (supporting); Writing – review & editing (supporting). **Junwen Zheng**: Funding acquisition (supporting); Validation (supporting). **Pan Wang**: Validation (supporting); Writing – original draft (supporting). **Longqun Ni**: Validation (supporting); Writing – original draft (supporting). **Xingyu Bao**: Validation (supporting); Writing – original draft (supporting). **Dandan Zhou**: Validation (supporting). **Bo Zhang**: Validation (supporting). **Kaibo Xiao**: Validation (supporting). **Handing Xia**: Formal analysis (supporting); Funding acquisition (supporting); Project administration (supporting); Resources (supporting); Supervision (supporting). **Rui Zhang**: Funding acquisition (supporting); Project administration (supporting); Resources (supporting); Supervision (equal). **Ping Li**: Formal analysis (supporting); Funding acquisition (equal); Project administration (supporting); Resources (supporting); Supervision (supporting); Validation (supporting); Writing – review & editing (equal). **Wanguo Zheng**: Funding acquisition (lead); Project administration (supporting); Resources (supporting); Supervision (equal); Validation (supporting). **Zinan Wang**: Conceptualization (lead); Formal analysis (equal); Funding acquisition (equal); Project administration (equal); Supervision (lead); Validation (supporting); Writing – review & editing (equal).

DATA AVAILABILITY

The data that support the findings of this study are available from the corresponding author upon reasonable request.

REFERENCES

[1]D. S. Montgomery, "Two decades of progress in understanding and control of laser plasma instabilities in indirect drive inertial fusion," Phys. Plasmas **23**, 055601 (2016).
[2]C. Labaune, "Incoherent light on the road to ignition," Nat. Phys. **3**, 680–682 (2007).
[3]S. H. Glenzer, D. H. Froula, L. Divol, M. Dorr, R. L. Berger, S. Dixit, B. A. Hammel, C. Haynam, J. A. Hittinger, J. P. Holder, O. S. Jones, D. H. Kalantar, O. L. Landen, A. B. Langdon, S. Langer, B. J. MacGowan, A. J. Mackinnon, N. Meezan, E. I. Moses, C. Niemann, C. H. Still, L. J. Suter, R. J. Wallace, E. A. Williams, and B. K. F. Young, "Experiments and multiscale simulations of laser propagation through ignition-scale plasmas," Nat. Phys. **3**, 716–719 (2007).
[4]J. Lindl, O. Landen, J. Edwards, and E. Moses, "Review of the National Ignition Campaign 2009-2012," Phys. Plasmas **21**, 020501 (2014).
[5]D. Veron, G. Thiell, and C. Gouedard, "Optical smoothing of the high power PHEBUS Nd-glass laser using the multimode optical fiber technique," Opt. Commun. **97**, 259–271 (1993).
[6]M. S. Pronko, R. H. Lehmberg, S. Obenschain, C. J. Pawley, C. K. Manka, and R. Eckardt, "Efficient second harmonic conversion of broad-band high-peak-power Nd:glass laser radiation using large-aperture KDP crystals in quadrature," IEEE J. Quantum Electron. **26**, 337–347 (1990).
[7]M. Nakatsuka, N. Miyanaga, T. Kanabe, H. Nakano, K. Tsubakimoto, and S. Nakai, "Partially coherent light sources for ICF experiment," Proc. SPIE **1870**, 151–162 (1993).
[8]S. I. Fedotov, L. P. Feoktistov, M. V. Osipov, and A. N. Starodub, "Lasers for ICF with a controllable function of mutual coherence of radiation," J. Russ. Laser Res. **25**, 79–92 (2004).
[9]M. Bowers, S. Burkhart, S. Cohen, G. Erbert, J. Heebner, M. Hermann, and D. Jedlovec, "The injection laser system on the National Ignition Facility," Proc. SPIE **6451**, 64511M (2007).
[10]A. Jolly, J.-F. Gleyze, D. Penninckx, N. Beck, L. Videau, and H. Coïc, "Fiber lasers integration for LMJ," C. R. Phys. **7**, 198–212 (2006).
[11]L. Hong-Huan, W. Jian-Jun, S. Zhan, L. Ming-Zhong, C. Guang-Hui, D. Lei, T. Jun, D. Qing-Hua, L. Yi-Ming, D. Yi-Fang, and L. Feng, "Integrated all fiber optical pulse generation system for laser fusion driver," Acta Phys. Sin. **57**, 1771 (2008).
[12]Department of Energy, DOE National Laboratory makes history by achieving fusion ignition, https://www.energy.gov/articles/doe-national-laboratory-makes-history-achieving-fusion-ignition, 2022.
[13]Y. Gao, L. Ji, X. Zhao, Y. Cui, D. Rao, W. Feng, L. Xia, D. Liu, T. Wang, H. Shi, F. Li, J. Liu, D. Pengyuan, X. Li, J. Liu, T. Zhang, C. Shan, Y. Hua, W. Ma, Z. Sui, J. Zhu, W. Pei, S. Fu, X. Sun, and X. Chen, "High-power, low-coherence laser driver facility," Opt. Lett. **45**, 6839 (2020).
[14]D. Rao, Y. Gao, Y. Cui, L. Ji, X. Zhao, J. Liu, D. Liu, F. Li, C. Shan, H. Shi, J. Liu, W. Feng, X. Li, W. Ma, and Z. Sui, "1 μJ nanosecond low-coherent laser source with precise temporal shaping and spectral control," Opt. Laser Technol. **122**, 105850 (2020).
[15]L. Ji, X. Zhao, D. Liu, Y. Gao, Y. Cui, D. Rao, W. Feng, F. Li, H. Shi, J. Liu, X. Li, L. Xia, T. Wang, J. Liu, P. Du, X. Sun, W. Ma, Z. Sui, and X. Chen, "High-efficiency second-harmonic generation of low-temporal-coherent light pulse," Opt. Lett. **44**, 4359 (2019).
[16]Y. Cui, Y. Gao, D. Rao, D. Liu, F. Li, L. Ji, H. Shi, J. Liu, X. Zhao, W. Feng, L. Xia, J. Liu, X. Li, T. Wang, W. Ma, and Z. Sui, "High-energy low-temporal-coherence instantaneous broadband pulse system," Opt. Lett. **44**, 2859 (2019).
[17]C. Dorrer, E. M. Hill, and J. D. Zuegel, "High-energy parametric amplification of spectrally incoherent broadband pulses," Opt. Express **28**, 451 (2020).
[18]C. Dorrer, M. Spilatro, S. Herman, T. Borger, and E. M. Hill, "Broadband sum-frequency generation of spectrally incoherent pulses," Opt. Express **29**, 16135 (2021).

[19]C. Dorrer and M. Spilatro, "Spectral and temporal shaping of spectrally incoherent pulses in the infrared and ultraviolet," Opt. Express **30**, 4942 (2022).
[20]J. W. Bates, J. F. Myatt, J. G. Shaw, R. K. Follett, J. L. Weaver, R. H. Lehmberg, and S. P. Obenschain, "Mitigation of cross-beam energy transfer in inertial-confinement-fusion plasmas with enhanced laser bandwidth," Phys. Rev. E **97**, 061202 (2018).
[21]Y. Zhao, S. Weng, M. Chen, J. Zheng, H. Zhuo, and Z. Sheng, "Stimulated Raman scattering excited by incoherent light in plasma," Matter Radiat. Extremes **2**, 190–196 (2017).
[22]S. K. Turitsyn, S. A. Babin, A. E. El-Taher, P. Harper, D. V. Churkin, S. I. Kablukov, J. D. Ania-Castañón, V. Karalekas, and E. V. Podivilov, "Random distributed feedback fibre laser," Nat. Photonics **4**, 231–235 (2010).
[23]D. V. Churkin, S. Sugavanam, I. D. Vatnik, Z. Wang, E. V. Podivilov, S. A. Babin, Y. Rao, and S. K. Turitsyn, "Recent advances in fundamentals and applications of random fiber lasers," Adv. Opt. Photonics **7**, 516 (2015).
[24]S. K. Turitsyn, S. A. Babin, D. V. Churkin, I. D. Vatnik, M. Nikulin, and E. V. Podivilov, "Random distributed feedback fibre lasers," Phys. Rep. **542**, 133–193 (2014).
[25]Z. Wang, H. Wu, M. Fan, L. Zhang, Y. Rao, W. Zhang, and X. Jia, "High power random fiber laser with short cavity length: Theoretical and experimental investigations," IEEE J. Sel. Top. Quantum Electron. **21**, 10–15 (2015).
[26]H. Zhang, L. Huang, J. Song, H. Wu, P. Zhou, X. Wang, J. Wu, J. Xu, Z. Wang, X. Xu, and Y. Rao, "Quasi-kilowatt random fiber laser," Opt. Lett. **44**, 2613 (2019).
[27]S. Lin, Z. Wang, Y. Qi, B. Han, H. Wu, and Y. Rao, "Wideband remote-sensing based on random fiber laser," J. Lightwave Technol. **40**, 3104–3110 (2022).
[28]H. Wu, H. Liu, W. Wang, Z. Wang, and H. Liang, "Tailoring the efficiency and spectrum of a green random laser generated by frequency doubling of random fiber lasers," Opt. Express **29**, 21521 (2021).
[29]S. A. Babin, A. E. El-Taher, P. Harper, E. V. Podivilov, and S. K. Turitsyn, "Tunable random fiber laser," Phys. Rev. A **84**, 021805 (2011).
[30]L. Zhang, H. Jiang, X. Yang, W. Pan, S. Cui, and Y. Feng, "Nearly-octave wavelength tuning of a continuous wave fiber laser," Sci. Rep. **7**, 42611 (2017).
[31]J. Xu, J. Ye, P. Zhou, J. Leng, H. Xiao, H. Zhang, J. Wu, and J. Chen, "Tandem pumping architecture enabled high power random fiber laser with near-diffraction-limited beam quality," Sci. China: Technol. Sci. **62**, 80–86 (2019).
[32]L. Zhang, H. Xie, Y. Li, F. Pang, W. Chen, L. Zhan, and T. Wang, "Towards optimal conversion efficiency of Brillouin random fiber lasers in a half-open linear cavity," Opt. Express **30**, 32097 (2022).
[33]S. Du, T. Qi, D. Li, P. Yan, M. Gong, and Q. Xiao, "10 kW fiber amplifier seeded by random fiber laser with suppression of spectral broadening and SRS," IEEE Photonics Technol. Lett. **34**, 721–724 (2022).
[34]L. Hu, D. He, H. Chen, X. Wang, T. Meng, L. Wen, J. Hu, Y. Xu, S. Li, Y. Chen, W. Chen, S. Chen, J. Tang, and B. Wang, "Research and development of neodymium phosphate laser glass for high power laser application," Opt. Mater. **63**, 213–220 (2017).
[35]H. Wu, B. Han, Z. Wang, and H. Liang, "Statistical properties of Er/Yb co-doped random Rayleigh feedback fiber laser," Chin. Opt. Lett. **19**, 021402 (2021).
[36]S. K. Turitsyn, A. E. Bednyakova, M. P. Fedoruk, A. I. Latkin, A. A. Fotiadi, A. S. Kurkov, and E. Sholokhov, "Modeling of CW Yb-doped fiber lasers with highly nonlinear cavity dynamics," Opt. Express **19**, 8394 (2011).
[37]S. V. Smirnov and D. V. Churkin, "Modeling of spectral and statistical properties of a random distributed feedback fiber laser," Opt. Express **21**, 21236 (2013).
[38]W. Zheng, X. Wei, Q. Zhu, F. Jing, D. Hu, X. Yuan, W. Dai, W. Zhou, F. Wang, D. Xu, X. Xie, B. Feng, Z. Peng, L. Guo, Y. Chen, X. Zhang, L. Liu, D. Lin, Z. Dang, Y. Xiang, R. Zhang, F. Wang, H. Jia, and X. Deng, "Laser performance upgrade for precise ICF experiment in SG-III laser facility," Matter Radiat. Extremes **2**, 243–255 (2017).
[39]M. Fan, Z. Wang, H. Wu, W. Sun, and L. Zhang, "Low-threshold, high-efficiency random fiber laser with linear output," IEEE Photonics Technol. Lett. **27**, 319–322 (2015).
[40]S. Gao, X. Xie, J. Tang, C. Fan, X. Fu, Z. Chen, and K. Yao, "Multi-beam large fundamental mode neodymium glass regenerative amplifier with uniform performance," Front. Phys. **10**, 923402 (2022).
[41]S. Lin, Z. Wang, Y. Qi, and Y. Rao, "*Long-distance random fiber laser sensing system with ultra-fast signal demodulation*," in *2022 Optical Fiber Communications Conference and Exhibition (OFC)* (IEEE, 2022), p. Th2A.13.
[42]J. Lindl, "Development of the indirect-drive approach to inertial confinement fusion and the target physics basis for ignition and gain," Phys. Plasmas **2**, 3933–4024 (1995).
[43]Y. Gao, Y. Cui, L. Ji, D. Rao, X. Zhao, F. Li, D. Liu, W. Feng, L. Xia, J. Liu, H. Shi, P. Du, J. Liu, X. Li, T. Wang, T. Zhang, C. Shan, Y. Hua, W. Ma, X. Sun, X. Chen, X. Huang, J. Zhu, W. Pei, Z. Sui, and S. Fu, "Development of low-coherence high-power laser drivers for inertial confinement fusion," Matter Radiat. Extremes **5**, 065201 (2020).
[44]S. Hüller and B. Afeyan, "Simulations of drastically reduced SBS with laser pulses composed of a Spike Train of Uneven Duration and Delay (STUD pulses)," EPJ Web Conf. **59**, 05010 (2013).